# Continuous segmented-flow synthesis of Ag and Au nanoparticles using a low-cost microfluidic PTFE tubing reactor

Gustavo Ochoa-Vazquez, Boris Kharisov, Ana Arizmendi-Morquecho, Anaïs Cario, Cyril Aymonier, Samuel Marre, Israel López

# Continuous segmented-flow synthesis of Ag and Au nanoparticles using a low cost microfluidic PTFE tubing reactor

Gustavo Ochoa-Vazquez, Boris Kharisov, Ana Arizmendi-Morquecho, Anaïs Cario, Cyril Aymonier, Samuel Marre, and Israel López*

***Abstract*— We present in here a simple and low cost continuous segmented-flow process for the synthesis of Ag and Au spherical-shaped nanoparticles. Different residence times (RT) were used to perform the nanoparticle synthesis, observing that at low RT, the Ag nanoparticles production, which uses a fast reduction reaction with $NaBH_4$, is improved due to an enhancement in the mixing of the reactants. However, the flow conditions have an opposite effect in the case of Au nanoparticles synthesis. Indeed, since the chemical reduction process (Turkevich method) exhibit a much slower kinetics, high RT (low flowrates) improve the synthesis yield and the quality of the nanoparticles. The Ag and Au nanoparticles were characterized by UV-Vis spectrophotometry (UV-Vis) and Transmission Electron Microscopy (TEM). The Ag spherical-shaped nanoparticles presented a LSPR at 400 nm (size ≈ 4 nm), while the synthesized Au nanoparticles exhibit LSPR and sizes in the range 520 - 550 nm and 14 - 17 nm, respectively.**

***Index Terms*— Ag nanoparticles, Au nanoparticles, Flow synthesis, Microfluidics, Microfluidic synthesis, Noble metal nanoparticles.**

This work was supported in part by the Consejo Nacional de Ciencia y Tecnologia of Mexico (CONACYT) under the Ph.D. Research scholarship of G. Ochoa-Vazquez (713466), and under the project CB-2017-2018-A1-S-39049. This work was supported by the European Research Council (ERC) through the European Union's Horizon 2020 Research and Innovation Program under Grant 725100 (project Big Mac). (Corresponding authors: Samuel Marre; Israel López.) G. Ochoa-Vazquez is with Universidad Autónoma de Nuevo León (UANL), Facultad de Ciencias Químicas (FCQ), Centro de Investigación en Biotecnología y Nanotecnología (CIBYN), Apodaca 66629, Mexico, and also with CNRS, Université Bordeaux, Bordeaux INP, ICMCB, UMR 5026, F-33600 Pessac, France. B. Kharisov is with Universidad Autónoma de Nuevo León (UANL), Facultad de Ciencias Químicas (FCQ), Centro de Laboratorios Especializados (CELAES), San Nicolás de los Garza 66455, Mexico. A. Arizmendi-Morquecho is with the Centro de Investigación en Materiales Avanzados, S. C. (CIMAV), Unidad Monterrey, Apodaca 66600, Mexico. A. Cario, C. Aymonier, and S. Marre are with CNRS, Université Bordeaux, Bordeaux INP, ICMCB, UMR 5026, F-33600 Pessac, France (e-mail: samuel.marre@icmcb.cnrs.fr). I. López is with Universidad Autónoma de Nuevo León (UANL), Facultad de Ciencias Químicas (FCQ), Centro de Investigación en Biotecnología y Nanotecnología (CIBYN), Apodaca 66629, Mexico (e-mail: israel.lopezhr@uanl.edu.mx).

## I. Introduction

In the last decade, Ag and Au nanoparticles (NPs) have been widely used in photonics [1], electronics [2], biomedicine [3] and catalysis [4] as well as in surface-enhanced Raman spectroscopy (SERS) for the design of nanostructured substrates [5] and chemical and biological sensors [6] thanks to their physical, chemical, optical and size-dependent properties [7].

Different synthesis methods have been employed to obtain these materials with distinct morphologies and sizes among which are electrochemical processes [8], photoreduction [9] or bio-assisted synthesis [10]. These approaches have permitted the obtention of several morphologies including nanospheres [11], nanorods [12] and nanotriangles [13] with sizes ranging from 4 nm to 100 nm [14]. Nevertheless, the most employed synthesis method remains the chemical reduction of metal precursors, which lead to the faster kinetics towards nanoparticle production [15]. Commonly, sodium borohydride ($NaBH_4$) is used as reducing agent in the Au and Ag nanoparticle synthesis for its potential reduction, while sodium citrate ($Na_3C_6H_5O_7 \cdot 2H_2O$ - $Na_3Cit$) is employed to stabilize the growth of the nanoparticles, producing spherical-shaped nanoparticles with sizes around 4-7 nm [16]. On the other hand, the Turkevich method [17] is the most used synthesis method of Au nanoparticles, obtaining spherical-shaped morphologies with sizes around 15-20 nm. In this synthesis recipe, $Na_3Cit$ is employed both as a reducing agent and as a stabilizer. These approaches are easily implemented in glasswares but suffered from irreproducibility from batch to batch given their sensitiveness to several factors such as mixing, concentration and temperature gradients, therefore requiring perfect control of the operating conditions [18].

Nowadays, the materials science community has been considering the use of flow chemistry - including microfluidic - as alternative to improve this kind of synthesis [19] due to the advantages offer by the small reaction volumes, the fast reaction rates, the rapid heat and mass transfer, the low operational costs [20], [21], and the possible parallelization and automation opportunities [22]. The microreactor can be fabricated with "on chip" configuration considering various materials depending on the reaction to be performed: polymers (PolyDimethylSiloxane), silicon, glass, metal or ceramics [23]. The inherent advantages of each materials (chemical

inertness, temperature and pressure stability, etc.) drives the choice of the technology to be employed [19]. Still, although microfabrication techniques have been democratized, making the microfabrication much easier than in the past, some know-how are generally still needed to proceed with on chip microdevices. Therefore, microreactors made out of simple tubings can also be considered. [24,25] Such configuration have – of course – much less flexibility in terms of designs than their on-chip counterparts provide; however, they are much more accessible by materials scientists given that all the required parts and equipment are commercially available. They provide cheap and simple approaches for continuous flow experiments with well-known hydrodynamics and easy manipulation of operating parameters (residence time, etc.).[26] In these plug-and-play modular configurations, the dimensions can be made similar to on chip microreactor (down to few tens of microns depending on the tubing dimensions), while providing opportunities to achieve facile scaling of developed processes for further larger scale production.[27]

Microfluidic synthesis of materials can be carried out in single phase [28] or segmented-flow, depending on the requirement of the synthesis [29] and the materials to be produced. While single-phase flows are easier to implement, they generally suffer from large residence time distribution (RTD) generated by dispersion effect in the flow. This generally results in large particles size distribution. Oppositely, segmented flows non only helps reducing RTD, but also favor mixing thanks to internal recirculation inside the flow, overcoming the classical diffusion-only mixing limitation in these low Reynolds number flows.[30]

Segmented flows are based on the generation of droplets or slugs separated by a carrier fluid (liquid-liquid or liquid-gas). Depending on the needs, the reaction can be carried out in the dispersed or the isolated phase. Such systems have been proved to improve the reproducibility and the control of materials synthesis reactions.[31]

In order to introduce flow chemistry to a larger community of materials scientists, we present in this paper a low cost approach using segmented-flow for the continuous synthesis of Ag and Au nanoparticles, using a simple reactor assembly of silica capillaries and PTFE. After introducing the reactor design and the chemical synthesis parameters, the optical and morphological characteristics of the obtained nanoparticles are dertermined, depending on the operating flow conditions.

## II. Materials and Methods

### A. Chemicals and solutions preparation

All the chemicals were purchased from Sigma Aldrich. $AgNO_3$ and $AuHCl_4 \cdot 3H_2O$ were used as metal precursors for each synthesis, and $NaBH_4$ as well as $Na_3Cit$ were employed as reducing agent on Ag and Au synthesis, respectively. All solution was prepared with 18.2 MΩcm-1 MilliQ water. Silicon oil (10 cSt @ 25 °C) was used as continuous phase Each reactor was covered to avoid any interaction between the ambient surrounding light and the light sensitive precursors. The droplet formation and segmented flow stability was monitored using an optical stereoscope.

For the Ag NPs synthesis, two different solutions were prepared: the precursor solution is 1 mM $AgNO_3$ and 5 mM $Na_3Cit$ in water, while the reducing solution is made out of $NaBH_4$ (8 mM in water), the latter being kept in an ice bath to avoid any $NaBH_4$ decomposition prior to use. For the Au NPs synthesis, the precursor solution contained $AuHCl_4 \cdot 3H_2O$ in water at a concentration of 0.25 mM, while the reducing solution is 34.5 mM $Na_3Cit$ in water. Both solutions were degassed before use.

### B. Tubing Reactor Fabrication and segmented flow synthesis conditions

The tubular reactor is composed of a transparent PTFE tubing (I.D. 0.03", O.D. 1/8") into which two silica capillaries (I.D. 100 µm, O.D. 200 µm) are inserted. A Y-shape Tee with bore hole diameters of 300 µm (IDEX©) serves at connecting the capillaries with the PTFE tube. The silica capillaries are connected to the Tee by the mean of short flangeless PEEK fittings and simple tubing sleeves, whose internal diameters match the external diameters of the capillaries. An additional Tee (IDEX©) in place downstream allowing the injection of the carrier fluid (silicon oil) and the creation of droplets based flow. The two reagent solutions (*i.e.* the Au or Ag precursor solution and the reducing reagent solution) are separately injected into each capillaries using KDS100 syringe pumps from KD Scientific equipped with 5 mL SGE® glass syringes. This ensures that the reaction only start at the droplets generation point, avoiding any clogging problem due to metal synthesis and deposition on the tubing wall. The length of the coiled tubing downstream the mixing / droplets generation point was adjusted depending on the metal nanoparticles synthesis process, *i.e.* 1 m (0.46 mL volume) and 1.9 m (0.87 mL volume) long for the Ag and the Au NPs synthesis, respectively, as each reaction does not require the same range of residence times.

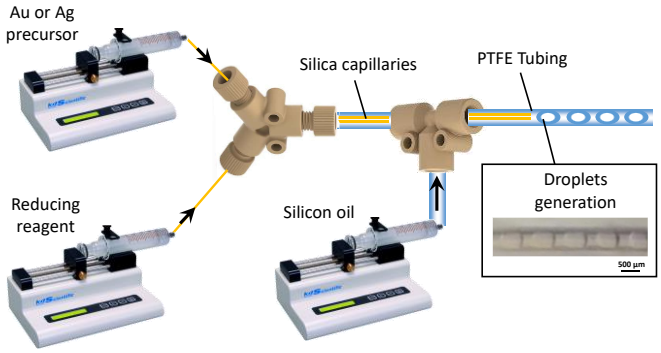


Fig. 1. Scheme of the tubing-based reactor employed for the continuous segmented flow synthesis of gold and Silver NPs.

We used equal flowrate for the [precursor / reducing solution] and the silicon oil, resulting in a 1:1 droplets / continuous phase segments volume fraction. When varying the residence time (by changing the overall flowrate) this condition was kept constant. For each sample, we waited at least the equivalent of three residence times before starting to collect the samples, in order to ensure a good stabilization of the droplets generation. At the outlet of the reactor, the products were collected directly in a 50 mL Pyrex beaker, where phase separation occurs (silicon oil being lighter than the aqueous phase).

**Silver NPs synthesis.** Ag NPs were synthesized at two different residence times, *i.e.* 0.6 (sample Ag-1) and 3 min (sample Ag-2). The utilized conditions are shown in Table I.

TABLE I.
FLOW RATE CONDITIONS FOR Ag NANOPARTICLES SYNTHESIS.

| Sample | Ag-1 | Ag-2 |
|---|---|---|
| **RT** | 0.6 min | 3 min |
| **Reactants** | Flow rates, Q (mL/h) | |
| **$AgNO_3$** | 17.6 | 3.5 |
| **$NaBH_4$** | 4.4 | 0.9 |
| **Silicone Oil** | 22 | 4.4 |
| **Qt (mL/h)** | 44 | 8.9 |

**Gold NPs synthesis.** Au NPs were synthesized using the Turkevich method adapted to flow conditions. To proceed with this method, the PTFE coiled tubing was immersed in an oil bath heated at 105 °C. Four different residence times were tested, namely: 3, 5, 10 and 20 min (samples Au-1, Au-2, Au-3 and Au-4). The operating conditions are listed in Table II.

TABLE II.
FLOW RATE CONDITIONS FOR Ag NANOPARTICLES SYNTHESIS.

| Lot | Au-1 | Au-2 | Au-3 | Au-4 |
|---|---|---|---|---|
| **RT** | 3 min | 5 min | 10 min | 20 min |
| **Reactants** | Flow rates, Q (mL/h) | | | |
| **$HAuCl_4$** | 4.2 | 2.6 | 1.3 | 0.65 |
| **$Na_3Cit$** | 4.2 | 2.6 | 1.3 | 0.65 |
| **Silicon Oil** | 8.4 | 5.2 | 2.6 | 1.3 |
| **$Q_t$ (mL/h)** | 16.8 | 10.4 | 5.2 | 2.6 |

The Ag and Au nanoparticle aqueous suspensions were recovered from the beaker and purified afterwards. The as synthesized NPs suspensions were centrifugated at 10,000 rpm for 20 min and further redispersed in milliQ water. This cleaning step was performed three times. Then, the redispersed NPs were stored at 4 °C in brown-colored glass vials, before their subsequent characterization.

### C. Apparatus and Measurements

The noble metal NP suspensions were characterized using a VARIAN Cary 5000 double-beam UV-Vis spectrophotometer, from 800 nm to 200 nm at room temperature. MilliQ water was employed as blank.

A JEOL JEM 2200FS FEG HR 200 kV electronic microscope was employed to determine the size and morphology of the nanoparticles. The samples were prepared by diluting in 2-propanol the corresponding NPs suspension several times, before placing some droplets on TEM grids. Statistical analysis of the obtained results was performed using Origin software and the image analysis was carried out using ImageJ and Gatan software out of at least 30 NPs measurements for each sample.

## III. Results and Discussion

### A. Ag nanoparticles

Fig. 3 shows the absorbance spectra of sample Ag-1 and Ag-2, respectively. The Ag-1 absorption spectrum displays the classical Local Surface Plasmon Resonance (LSPR) signal for spherical-shaped Ag NPs, < 20 nm, at $\lambda$ = 400 nm [32]. This LSPR signal is related with the coherent collective oscillation of the valence electrons in the metal NPs and it depends on their size and shape [33]. On the other hand, sample Ag-2 shows a mean LSPR signal at $\lambda$ = 418 nm and a secondary signal at $\lambda$ = 569 nm, which could be attributed to the formation of Ag NPs with sizes from 45 (most) to 100 nm (minority). Besides, the maximum absorption for Ag-1 is more than 50 times greater than Ag-2, this difference is attributed to the higher conversion yield for the Ag-1 conditions.

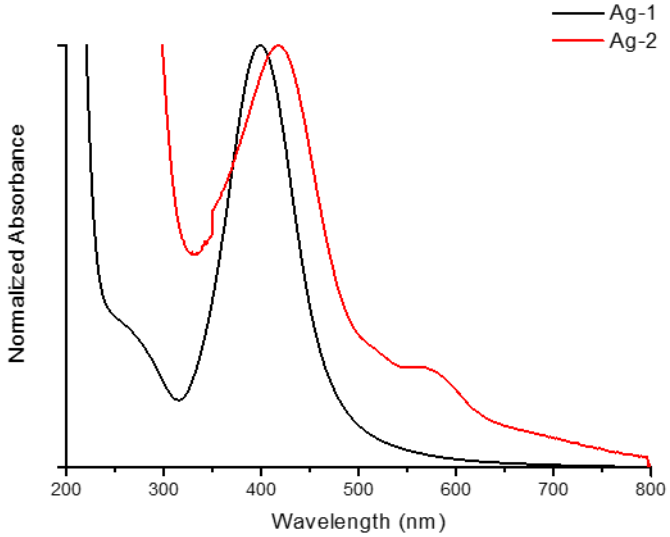


Fig. 3. Normalized (1x black 56x red) UV-Vis spectra of Ag NPs suspensions for samples Ag-1 RT = 0.6 min) and Ag-2 (RT = 3 min).

Fig. 4a show the Ag NPs obtained at 0.6 min of RT (Ag-1), observing spherical morphologies of 4.2 ± 1.4 nm of size. Nevertheless, it can also be seen that larger particles (Figure 4b) are also present, generating polydispersity (Fig. 4c). This effect could be due to potential interactions between the $Na_3Cit$ and the silicon oil continuous phase. Since $Na_3Cit$ can act as a surfactant, it may stabilize some silicon oil inside the aqueous phase, altering the chemical reaction and therefore the growth of the Ag NPs [34]. Additionally, the used of $NaBH_4$ as a reducing reagent generate hydrogen, which cannot be extracted from the liquid / liquid segmented flow. This generated hydrogen might also affect the chemical reaction, and consequently the growth mechanisms of nanoparticles [35]. The use of a three-phase flow (liquid / liquid /gas) could therefore be considered to solve this problem, as reported in the literature. [Adrian M Nightingale, Thomas W Phillips, James H Bannock, John C De Mello, Controlled multistep synthesis in a three-phase droplet reactor, Nature Comm.,

2014, 5(1), 1-8]

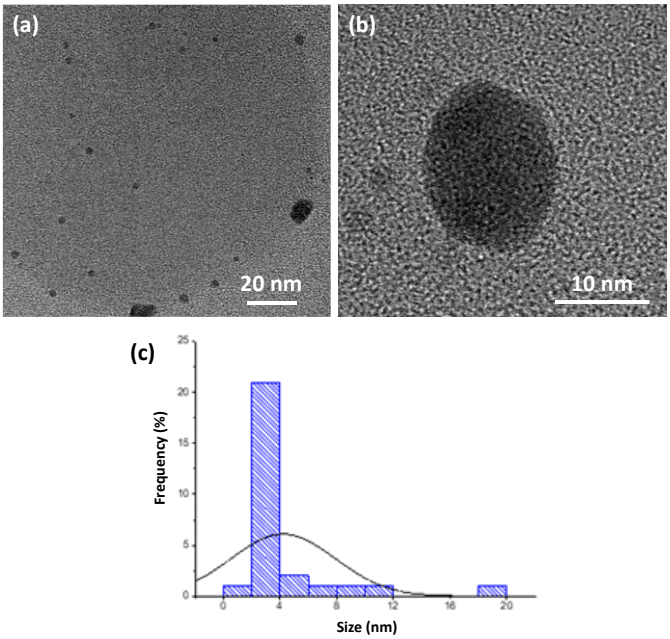


Fig. 4. TEM images of Ag nanoparticles obtained at 0.6 min of RT. a) TEM image of Ag nanoparticles surrounding an oil droplet. b) Zoomed TEM image of Ag nanoparticle and oil droplet in decomposition. c) size distribution graph of Ag nanoparticles showed in a).

In contrast with sample Ag-1, sample Ag-2 did not produce enough amount of Ag nanoparticles to be characterized by means of TEM. However, based on the UV-Vis absorption spectrum, it can be mentioned that larger polydispersity is present. This behavior could be attributed to the flow conditions at larger RT. By increasing the RT (and therefore reducing flow rates), the shear stress decreases, hindering the fluid deformation and, consequently the mixing process inside the droplets [36]. The mixing is critical in this fast reduction reaction since multiple nucleation steps can occur if the reagents are not quickly mixed together, resulting in large particles size distribution.

### *B. Au nanoparticles*

Gold nanoparticles were synthesized at different flowrates, maintaining all the other parameters constant such as the temperature of the oil bath (105 °C) and the $HAuCl_4$ : $Na_3Cit$ flowrates ratio at 1:1 (resulting in a concentration ratio of 1:138).

Fig 5 shows the absorption spectra of samples Au-1 through Au-4. Two effects can be noticed. First, higher RT results in an increase of the absorbance intensity, which can be directly related to a higher concentration of Au NPs. Second, we can observed a blue shift coupled to a narrowing of the LSPR with an increasing residence time. This can be explained by a narrowing of the particle size distribution at longer residence times, resulting in an improvement of the Au NPs optical properties.

This could be related to the RT of the fluid. At lower RT, the fluid is not heated as fast as the chemical reaction needs, disadvantaging the Au nanoparticle obtention. On the other hand, at higher RT, the fluid has enough time to warm up therefore allowing the reduction of $Au^{3+}$ to $Au^0$ and stabilizing the nanoparticles, thus improving the Au nanoparticles production [37].

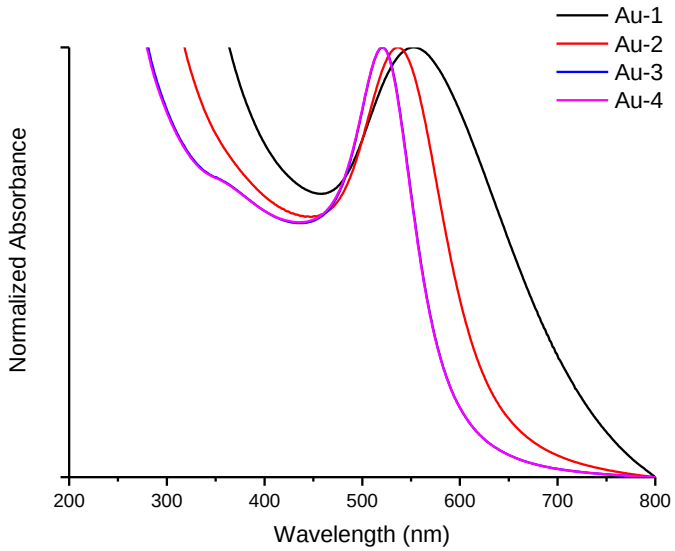


Fig. 5. UV-Vis absorbance spectra of Au nanoparticles suspension obtained at 3, 5, 10 and 20 min of RT (samples Au-1 through Au-4, respectively.).

Considering the short residence times (samples Au-1 and Au-2), sample Au-1 presents the lowest absorbance and a red-shifted LSPR at 550 nm. This could be related to low reaction control due to mixing and heating problems previously explained as well as bigger nanoparticles sizes, scattering lighter because of a larger optical cross-section [39]; non-spherical morphologies [40] and nanoparticle aggregations [41] (Fig.8a). Oppositely, thanks to slightly longer RT, sample Au-2 presents a LSPR at 540 nm, nanoparticles with spherical morphologies and non-aggregation problems, as is observed in Fig 8b. Neverthless, in all TEM images, is possible to observe impurities regarding to oil droplet traces, hindering to zoom in the sample.

Concerning the longer residence times, the characteristic LSPR of Au spherical-shaped nanoparticles at 520 nm in the samples Au-3 and Au-4, indicates nanoparticle sizes around 15-18 nm [36]. This is confirmed by the TEM measurements (Fig. XXX and Fig. XXX) showing spherical Au NPs with average sizes of 16.2 ± 0.6 and 15 ± 0.6 nm, respectively.

However, other morphologies can also be noticed. This could be attributed to the presence of light in the synthesis [38], even if the reactor was covered. On the other hand, the Fig. 7a indicates the characteristic crystal planes (111), (200), (220) and (311) for metallic gold. Also, Fig. 7b shows that the samples obtained are polycrystalline.

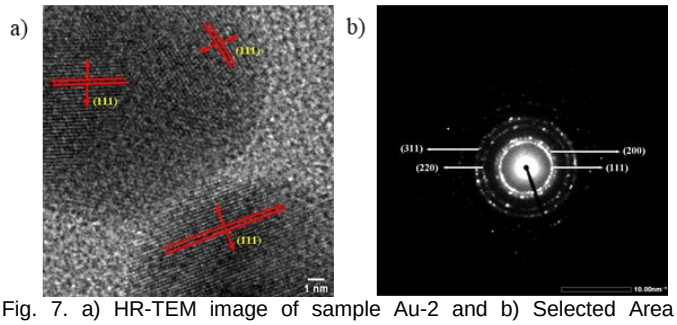


Fig. 7. a) HR-TEM image of sample Au-2 and b) Selected Area Electron Diffraction (SAED).

Fig. 8. TEM images of a) LotB2 and b) LotC2. Size distribution chart of c) LotB2 and d) LotC2.

Finally, Fig. 5. Shows a characteritic absorbance band that narrows when the RT increase, demonstrating the improvement of the monodispersity of the nanoparticles [42]. The Fig. 6c, 6d, 8c, and 8d show the increase in the nanoparticle monodispersity when the RT goes from 3 min to 20 min, agreeing with the observed in the UV-Vis spectra.

## V. Conclusions

After all the experiments realized and the results obtained in this work is possible to conclude that, in accordance with Ag nanoparticle synthesis, 0.6 min of RT produce nanoparticles of 7 nm with spherical-shaped morphology, characteristic to LSPR at 400 nm. However, 3 min of RT did not produce Ag nanoparticles.

For Au nanoparticle synthesis, RT at 3 min generate Au nanoparticles with high polydispersity, nanoparticle agglomeration and red-shifted Au LSPR at 550 nm. 5, 10 and 20 min of RT produce Au spherical-shaped nanoparticles. This last two conditions generate Au nanoparticles of 16.5 and 17 nm, respectively, typically sizes of the LSPR at 520 nm observed. This demonstrate that increasing RT improves the production of these nanoparticles and their monodispersity.

For each tubing reactor (1.9 m) the Au NPs production rate, at the Au-3 condition, is 31.4 mg per day.

High er T ➔ increase kinetics ➔ lower RT required ➔ higher production

## VI. References

[1] L. R. P. Kassab and C. B. De Araujo, Metal nanostructures for photonics. Elsevier, 2018.)

[2] B. Xue, P. Chen, Q. Hong, J. Lin, and K. L. Tan, “Growth of Pd, Pt, Ag and Au nanoparticles on carbon nanotubes,” J. Mater. Chem., vol. 11, pp. 2378–2381, 2001.

[3] F. Caruso, T. Hyeon, and V. Rotello, “Nanomedicine themed issue,” Chem. Soc. Rev., vol. 41, no. 7, pp. 2740–2779, 2012.

[4] P. Hervés et al., “Catalysis by metallic nanoparticles in aqueous solution: model reactions w,” Chem. Soc. Rev., vol. 41, no. 17, pp. 5569–5868, 2012.

[5] C. Puente, M. Sánchez-Domínguez, C. L. Brosseau, and I. López, “Silver-chitosan and gold-chitosan substrates for surface-enhanced Raman spectroscopy (SERS): Effect of nanoparticle morphology on SERS performance,” Mater. Chem. Phys., vol. 260, no. August 2020, 2021.

[6] M. Mitsushio, K. Miyashita, and M. Higo, “Sensor properties and surface characterization of the metal-deposited SPR optical fiber sensors with Au, Ag, Cu, and Al,” Sensors Actuators A. Phys., vol. 125, pp. 296–303, 2006.

[7] B. Xue, P. Chen, Q. Hong, J. Lin, and K. L. Tan, “Growth of Pd, Pt, Ag and Au nanoparticles on carbon nanotubes,” J. Mater. Chem., vol. 11, pp. 2378–2381, 2001.

[8] J. Bakhsh, R. Ojani, E. Hasheminejad, and S. Rashid-nadimi, “Applied Surface Science Electrochemical synthesis of Ag nanoparticles supported on glassy carbon electrode by means of p - isopropyl calix [6] arene matrix and its application for electrocatalytic reduction of H2O2,” Appl. Surf. Sci., vol. 258, no. 7, pp. 2788–2795, 2012.

[9] C. Li et al., “Shaped femtosecond laser induced photoreduction for highly controllable Au nanoparticles based on localized field enhancement and their SERS applications,” Nanophotonics, vol. 9, no. 3, pp. 691–702, 2020.

[10] C. Tamuly, M. Hazarika, S. Ch, M. R. Das, and M. P. Boruah, “In situ biosynthesis of Ag, Au and bimetallic nanoparticles using Piper pedicellatum C. DC: Green chemistry approach,” Colloids Surfaces B Biointerfaces, vol. 102, pp. 627–634, 2013.

[11] P. Y. Lim, “Synthesis of Ag nanospheres particles in ethylene glycol by electrochemical-assisted polyol process,” Chem. Phys. Lett., vol. 420, pp. 304–308, 2006.

[12] R. Becker, B. Liedberg, and P. Käll, “CTAB promoted synthesis of Au nanorods – Temperature effects and stability considerations,” J. Colloid Interface Sci., vol. 343, no. 1, pp. 25–30, 2010.

[13] A. Rai, M. Chaudhary, A. Ahmad, S. Bhargava, and M. Sastry, “Synthesis of triangular Au core – Ag shell nanoparticles,” Mater. R, vol. 42, pp. 1212–1220, 2007.

[14] Y. Sakka and A. Overview, “A review on the classification, characterization, synthesis of nanoparticles and their application A review on the classification, characterization, synthesis of nanoparticles and their application,” IOP Conf. Ser. Mater. Sci. Eng., vol. 263, no. 3, pp. 1–15, 2017.

[15] K. Gudikandula and S. C. Maringanti, “Synthesis of silver nanoparticles by chemical and biological methods and their antimicrobial properties,” J. Exp. Nanosci., vol. 11, no. 9, pp. 714–721, 2016.

[16] K. Mavani and M. Shah, “Synthesis of Silver Nanoparticles by using Sodium Borohydride as Redusing Agent,” IJERT, vol. 2, no. 3, pp. 1–5, 2013.

[17] M. Wuithschick et al., “Turkevich in New Robes: Key Questions Answered for the Most Common Gold Nanoparticle Synthesis,” ACS Nano, vol. 9, no. 7, pp. 7052–7071, 2015).

[18] S. S. Shankar, A. Rai, A. Ahmad, and M. Sastry, “Rapid synthesis of Au, Ag, and bimetallic Au core – Ag shell nanoparticles using Neem ( Azadirachta indica ) leaf broth,” J. Colloid Interface Sci., vol. 275, pp. 496–502, 2004.

[19] S. Marre and K. F. Jensen, “Synthesis of micro and nanostructures in microfluidic systems,” Chem. Soc. Rev., vol. 39, no. 3, pp. 1183–1202, 2010.

[20] N.-T. Nguyen, S. T. Wereley, and S. A. M. Shaegh, Fundamentals and applications of microfluidics. Artech house, 2019.

[21] G. M. Whitesides, “The origins and the future of microfluidics,” Nature, vol. 442, no. 7101. pp. 368–373, 27-Jul-2006.

[22] N. Convery and N. Gadegaard, “Micro and Nano Engineering 30 years of micro fl uidics,” Micro Nano Eng., vol. 2, no. November 2018, pp. 76–91, 2019.

[23] G. Ochoa-Vazquez et al., “Microfluidics and Surface-Enhanced Raman Spectroscopy: A Perfect Match for New Analytical Tools,” IEEE Trans. Nanobioscience, vol. 18, no. 4, pp. 558–566, 2019.

[24] K. S. Elvira, X. Casadevall, R. C. R. Wootton, and J. Andrew, “The past, present and potential for microfluidic reactor technology in chemical synthesis,” Nat. Chem., vol. 5, no. October, pp. 905–915, 2013.

[25] A. M. Nightingale et al., “A stable droplet reactor for high temperature nanocrystal synthesis,” Lab Chip, vol. 11, no. 7, pp. 1221–1227, 2011.
[26] H. Nakamura, Y. Yamaguchi, M. Miyazaki, H. Maeda, M. Uehara, and P. Mulvaney, “Preparation of CdSe nanocrystals in a micro-flow-reactor,” Chem. Commun., vol. 23, pp. 2844–2845, 2002.
[27] A. M. Nightingale et al., “Large-scale synthesis of nanocrystals in a multichannel droplet reactor,” J. Mater. Chem. A, vol. 1, no. 12, pp. 4067–4076, 2013.
[28] J. Yoshida, A. Nagaki, and D. Yamada, “Continuous flow synthesis,” Drug Discov. Today Technol., vol. 10, no. 1, pp. e53–e59, 2013.
[29] M. Abolhasani and K. F. Jensen, “Oscillatory multiphase flow strategy for chemistry and biology,” Lab Chip, vol. 16, pp. 2775–2784, 2016.
[30] M. T. Kreutzer, A. Günther, and K. F. Jensen, “Sample dispersion for segmented flow in microchannels with rectangular cross section,” Anal. Chem., vol. 80, no. 5, pp. 1558–1567, 2008.
[31] J. M. Köhler and A. Knauer, “Why is Micro Segmented Flow Particularly Promising for the Synthesis of Nanomaterials?”, Chem. Eng. Technol., no. 6, pp. 887–899, 2013.)
[32] E. Nourafkan and A. Alamdari, “Study of effective parameters in silver nanoparticle synthesis through method of reverse microemulsion,” J. Ind. Eng. Chem., vol. 20, no. 5, pp. 3639–3645, 2014.
[33] D. Paramelle, A. Sadovoy, S. Gorelik, P. Free, J. Hobley, and D. G. Fernig, “A rapid method to estimate the concentration of citrate capped silver nanoparticles from UV-visible light spectra,” Analyst, vol. 139, no. 19, pp. 4855–4861, 2014.
[34] L. Xu, J. Peng, M. Yan, D. Zhang, and A. Q. Shen, “Chemical Engineering and Processing: Process Intensi fi cation Droplet synthesis of silver nanoparticles by a micro fl uidic device,” Chem. Eng. Process. Process Intensif., vol. 102, pp. 186–193, 2016.
[35] L. Lu and X. An, “Silver nanoparticles synthesis using H2 as reducing agent in toluene-supercritical CO2 microemulsion,” J. Supercrit. Fluids, vol. 99, pp. 29–37, 2015.
[36] A. Enders, I. G. Siller, K. Urmann, M. R. Hoffmann, and J. Bahnemann, “3D Printed Microfluidic Mixers—A Comparative Study on Mixing Unit Performances,” Small, vol. 15, no. 2, pp. 1–9, 2019.
[37] V. S. Cabeza, S. Kuhn, A. A. Kulkarni, and K. F. Jensen, “Size-Controlled Flow Synthesis of Gold Nanoparticles Using a Segmented Flow Micro fl uidic Platform,” Langmuir, vol. 28, pp. 7007–7013, 2012.
[38] P. N. Njoki et al., “Size Correlation of Optical and Spectroscopic Properties for Gold Nanoparticles,” J.Phys. Chem. C, vol. 111, pp. 14664–14669, 2007.
[39] L. Scarabelli, M. Coronado-puchau, J. J. Giner-casares, J. Langer, and L. M. Liz-marza, “Monodisperse Gold Nanotriangles: Assembly, and Performance in Surface-Enhanced Raman Scattering,” ACS Nano, vol. 8, no. 6, pp. 5833–5842, 2014.
[40] M. Grzelczak, J. Pe, and L. M. Liz-marza, “Shape control in gold nanoparticle synthesis w,” Chem. Soc. Rev., vol. 37, pp. 1783–1791, 2008.
[41] C. Tserkezis, R. W. Taylor, J. Beitner, R. Esteban, J. J. Baumberg, and J. Aizpurua, “Optical Response of Metallic Nanoparticle Heteroaggregates with Subnanometric Gaps,” Part. Part. Syst. Charact., vol. 31, pp. 152–160, 2014.
[42] L. Sun, W. Luan, Y. Shan, and S. Tu, “One-step synthesis of monodisperse Au – Ag alloy nanoparticles in a microreaction system,” Chem. Eng. J., vol. 189–190, pp. 451–455, 2012.